

Epitaxial growth mechanisms and structure of $\text{CaF}_2/\text{Si}(111)$

C. A. Lucas, D. Loretto, and G. C. L. Wong*

Materials Sciences Division, Lawrence Berkeley Laboratory, University of California, Berkeley, California 94720

(Received 1 April 1994; revised manuscript received 16 June 1994)

The early stages of interface formation between CaF_2 and $\text{Si}(111)$ have been studied, *in situ*, by a combination of reflection high-energy electron diffraction, x-ray diffraction, and core-level photoemission. The results are combined with *ex situ* transmission-electron-microscopy measurements to show that the initial growth mode changes from Volmer-Weber to Stranski-Krastanow, depending on the substrate temperature. The crossover is correlated with a submonolayer transition from the $\text{Si}(111)$ - (7×7) to a (3×1) reconstruction. This is accompanied by fluorine dissociation at the interface. Both initial growth modes can lead to a uniform CaF_2 epilayer and subsequent growth on this surface is layer by layer. Using x-ray crystal truncation-rod analysis, we have examined the $\text{CaF}_2/\text{Si}(111)$ surface and interface structure. For films grown at temperatures above the $(7\times 7)\rightarrow(3\times 1)$ transition, the Ca atom in the CaF layer at the interface is located in a single T_4 bonding site. Finally, we have observed a structural transition at the interface from the as-grown structure to a $(\sqrt{3}\times\sqrt{3})R30^\circ$ reconstruction, which appears to be incommensurate. The dynamics of this transition and the possible mechanisms will be discussed.

I. INTRODUCTION

CaF_2/Si is a prototypical ionic/covalent system with a lattice mismatch of only 0.6% at room temperature. As a result, $\text{CaF}_2/\text{Si}(111)$ has been studied both theoretically and experimentally and is a prime candidate for technological application in semiconductor on insulator devices.¹ The early stages of interface formation have been studied with x-ray photoelectron spectroscopy (XPS),^{2,3} medium-energy ion scattering (MEIS),⁴ scanning tunneling microscopy (STM),⁵ and x-ray standing-wave (XSW) measurements.⁶ It has been concluded that CaF_2 dissociates to give CaF at the interface and various ordered CaF -Si structures have been observed at submonolayer coverages. From a MEIS study of monolayer coverages, Tromp and Reuter proposed a T_4 bonding site for the Ca atom in the CaF layer.⁴ In contrast, Zegenhagen and Patel observed a mixture of three distinct bonding sites in submonolayer coverages, depending on the substrate temperature.⁶ At higher temperatures, an equal occupation of T_4 and H_3 sites gave the best agreement with their XSW measurements.

In early papers the growth mechanism of CaF_2 on the CaF layer was often assumed to be layer by layer. Recently a composite growth mode has been observed in a combined core-level photoemission/transmission-electron-microscopy (TEM) study⁷ and was also inferred from x-ray photoelectron diffraction results.⁸ This is best described as a Stranski-Krastanow pathway to layer-by-layer growth, beginning with CaF_2 coherent island formation on the Si- CaF layer and then layer by layer CaF_2 homoepitaxy.

The interface structure in thicker epitaxial $\text{CaF}_2/\text{Si}(111)$ films has also been controversial. Batstone, Phillips, and Hunke proposed an on-top site for the interfacial Ca atom on the basis of image simulation of high-resolution transmission-electron-microscopy (HRTEM)

results.⁹ X-ray diffraction measurements, however, appeared to confirm the submonolayer XSW studies, with the H_3/T_4 mixture causing a domain structure in the CaF_2 film.¹⁰ Recently, we observed a structural transition at the interface, depending critically on the CaF_2 overlayer thickness.¹¹

In this paper we present a comprehensive study of $\text{CaF}_2/\text{Si}(111)$ heteroepitaxy, from the early stages of interface formation to the structure and stability of thicker epitaxial films. The results reveal the temperature dependence of the submonolayer structures that are formed and their influence on the growth modes and subsequent interface structures. Our results explain many of the discrepancies between previous experimental studies and provide a basis for theoretical structural calculations. We also reexamine the interface transition and suggest a mechanism based on defect diffusion in the ionic overlayer.

The paper is structured as follows. In Sec. II we give the details of sample preparation and the different experimental techniques. In Sec. III we present results of *in situ* reflection high-energy electron-diffraction (RHEED), x-ray-diffraction, and XPS measurements aimed at understanding the ordering in the submonolayer regime. These results are combined with *ex situ* TEM measurements to demonstrate the different growth mechanisms which lead to pseudomorphic, epitaxial CaF_2 films. In Sec. IV x-ray diffraction is used to probe the interface structures that result from the different initial growth temperatures. We also present a combined x-ray diffraction/TEM study of the CaF_2/Si interface structure formed at high substrate temperatures. Interpretation of the x-ray-diffraction measurements reveals that the interface Ca atom is located at a single T_4 site. The combination of real-space and reciprocal-space techniques is a powerful method for studying the structure of epitaxial films and their buried interfaces. In Sec. V we describe the metastability of the

as-formed $\text{CaF}_2/\text{Si}(111)$ interface and its transition to a new interface structure. Finally, Sec. VI summarizes the results and highlights some possible developments.

II. EXPERIMENTAL DETAILS

CaF_2 was grown by molecular-beam epitaxy (MBE) on well-oriented (miscut $<0.5^\circ$) $\text{Si}(111)$ substrates in a three-chamber ISA/Riber ultrahigh vacuum (UHV) system. Full details of the sample preparation and vacuum system have been given previously.^{7,11,12} CaF_2 was evaporated from a boron nitride effusion cell at 1150°C (corresponding to a deposition rate of $\sim 30 \text{ \AA}$ per minute during the initial stages of growth) with the sample being held at the desired substrate temperature T as measured by a W/Re thermocouple. The thermocouple calibration can be referenced to the $\text{Si}(1\times 1)\rightarrow(7\times 7)$ phase transition,¹³ obtained on slow cooling of the sample, and was observed by RHEED to occur at $T\sim 870\text{--}880^\circ\text{C}$.¹⁴ After growth, samples were removed from the vacuum for *ex situ* TEM and x-ray scattering studies or transferred under vacuum to an analysis chamber for XPS measurements. Some samples, particularly those with low coverages of CaF_2 , were capped with a thin ($50\text{--}100 \text{ \AA}$) layer of amorphous Si. TEM measurements were performed at a voltage of 200 keV in JEOL 200 CX microscopes. X-ray diffraction measurements were performed using a Huber four-circle diffractometer based on a Rigaku 12-kW rotating anode x-ray source.¹² Additional x-ray scattering measurements were performed on beam line 7-2 at the Stanford Synchrotron Radiation Laboratory (SSRL), with a focused 1 mm (vertical plane) \times 2 mm (horizontal) incident x-ray beam ($\lambda=1.24 \text{ \AA}$).

In Sec. III we also present some x-ray-diffraction measurements performed on beam line X16A at the National Synchrotron Light Source (NSLS), Brookhaven National Laboratory, using an *in situ* UHV chamber coupled to a five-circle diffractometer. In-plane x-ray-diffraction measurements were performed in a grazing incidence geometry with a focused $1.0 \text{ mm} \times 1.5 \text{ mm}$ incident beam ($\lambda=1.37 \text{ \AA}$). In this geometry, the incident angle of the x-ray beam to the sample surface was equal to the exit angle $\beta=0.61^\circ$, which is well above the critical angle for total external reflection from the Si substrate. Full details of the diffractometer design and instrumental resolution have been given elsewhere.¹⁵

III. THE RELATIONSHIP BETWEEN SUBMONOLAYER STRUCTURE AND GROWTH MODES

During CaF_2 deposition the (7×7) RHEED pattern of the clean $\text{Si}(111)$ surface changes to a (1×1) pattern. At $T>550^\circ\text{C}$ the pattern evolves in the sequence $(7\times 7)\rightarrow(3\times 1)\rightarrow(4\times 1)\rightarrow(1\times 1)$. At $T<450^\circ\text{C}$ the (7×7) gradually fades to a (1×1) pattern and (3×1) and (4×1) patterns are not observed. These results suggest that the initial stages of $\text{CaF}_2/\text{Si}(111)$ deposition are two-dimensional at high temperatures, since a small amount of CaF_2 flux completely transforms the (7×7) to a (3×1) surface, and three-dimensional at low temperatures, since a much larger amount of material weakens, but does not

remove, the (7×7) RHEED pattern.¹⁶ At $T\sim 500^\circ\text{C}$ a superposition of (3×1) , (4×1) , and (7×7) RHEED patterns precedes the appearance of a (1×1) pattern.

In situ grazing incidence x-ray diffraction allows a quantitative measure of the intensities and line shapes of the superlattice Bragg reflections observed by RHEED. The $(\frac{3}{7}, 0)$ and $(\frac{1}{3}, 0)$ surface Bragg reflections [indexed using the standard two-dimensional low-energy electron-diffraction (LEED) notation for the $\text{Si}(111)$ hexagonal surface unit cell] are specific to the (7×7) and (3×1) reconstructions, respectively. Figure 1(a) shows rocking scans (rotation about the surface normal) through the $(\frac{3}{7}, 0)$ reflection. The solid lines are fits to the data using a Lorentzian line shape which enables the peak intensity and full width at half maximum (FWHM) to be obtained. For the clean surface, before CaF_2 deposition [triangular symbols in Fig. 1(a)], the FWHM corresponds to an aver-

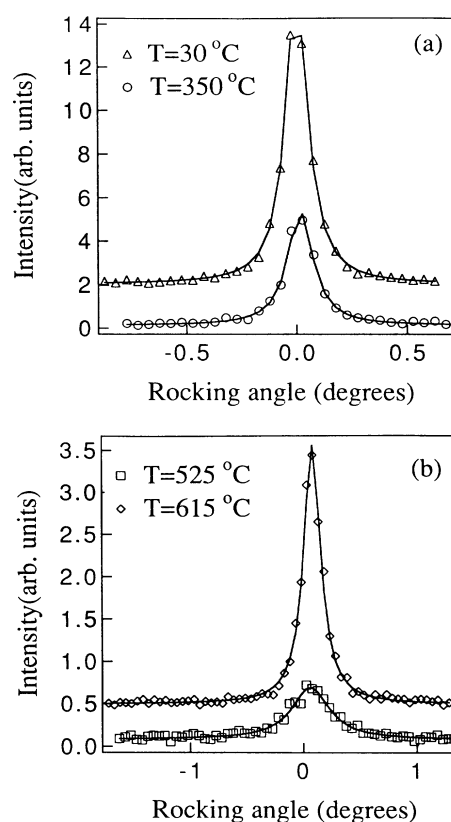


FIG. 1. X-ray rocking scans through the (a) $(\frac{3}{7}, 0)$ and (b) $(\frac{1}{3}, 0)$ superlattice Bragg reflections which are due to the $\text{Si}(7\times 7)$ and $\text{CaF-Si}(3\times 1)$ reconstructions, respectively. In (a) one set of data was taken from the clean Si surface and the other was taken after CaF_2 deposition and at a substrate temperature $T\sim 350^\circ\text{C}$. In (b) the data were taken at $T=525^\circ\text{C}$, at the onset of the $(7\times 7)\rightarrow(3\times 1)$ transition, and at $T=620^\circ\text{C}$, where the transition is complete. In both (a) and (b) the data sets have been displaced for clarity and the solid lines are calculated Lorentzian line shapes with a constant background level. The fitted line shapes were used to obtain the peak intensities and widths described in the text and the integrated intensities in Fig. 2.

age correlation length L of ~ 3600 Å. This is consistent with domain boundaries at steps on the surface, the distribution being determined by the sample miscut ($< 0.5^\circ$). Deposition of CaF_2 on the $\text{Si}(111)$ surface at room temperature caused no appreciable change in the intensity or width of the $(\frac{3}{7}, 0)$ peak [the amount of material deposited was equal to the amount that gave a (3×1) reconstruction at a substrate temperature of $\sim 700^\circ\text{C}$ in a prior deposition experiment]. As the sample was heated above room temperature there was a dramatic decrease in the intensity of the $(\frac{3}{7}, 0)$ reflection. The rocking scan through the $(\frac{3}{7}, 0)$ peak at $T = 350^\circ\text{C}$ is also shown in Fig. 1(a). The width of the peak corresponds to only a slight decrease in the correlation length $L \sim 3200$ Å, although there is nearly a 50% decrease in the integrated intensity.¹⁷ At this temperature there was still no intensity at $(\frac{1}{3}, 0)$, in agreement with RHEED, which indicated that the $(7 \times 7) \rightarrow (3 \times 1)$ transition occurs at $\sim 500^\circ\text{C}$. At $T \sim 510^\circ\text{C}$, intensity began to appear at the $(\frac{1}{3}, 0)$ superlattice reflection. Rocking scans through $(\frac{1}{3}, 0)$ are shown for two sample temperatures in Fig. 1(b). Again, the fits to the data are Lorentzian line shapes and at the higher temperature the FWHM corresponds to a correlation length $L = 3200$ Å. Figure 2 summarizes the temperature dependence of integrated intensity for both the $(\frac{3}{7}, 0)$ and $(\frac{1}{3}, 0)$ surface reflections. There is a clear crossover in intensity from $(\frac{3}{7}, 0)$ to $(\frac{1}{3}, 0)$ indicating that the (3×1) domains are forming at the expense of the $\text{Si}(7 \times 7)$. The width behavior of the $(\frac{1}{3}, 0)$ peak indicates that the (3×1) domain size grows rapidly at the onset of the transition. As the integrated intensity of the $(\frac{1}{3}, 0)$ reflection increases we can conclude that the transition is not equivalent to an "order-disorder" transition on the surface. In addition, the transition is irreversible, as cool-

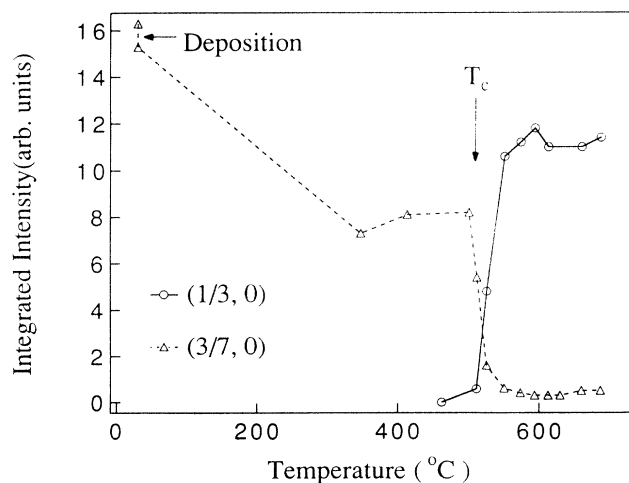


FIG. 2. The temperature dependence of the integrated intensities of the $(\frac{3}{7}, 0)$ and $(\frac{1}{3}, 0)$ superlattice Bragg reflections. Very little change is observed after CaF_2 deposition at room temperature. At $T \sim 500^\circ\text{C}$ the surface undergoes a transition to an ordered (3×1) structure which appears to wet the Si substrate and completely remove the (7×7) reconstruction.

ing the sample to room temperature caused no decrease in the $(\frac{1}{3}, 0)$ peak intensity.

Figure 3 shows the $\text{Ca } 2p$ XPS spectra for a submonolayer coverage of CaF_2 at three different sample temperatures. In Fig. 3(a) the data are obtained after deposition at room temperature [RHEED showed a faded (7×7) pattern]. The data in Fig. 3(b) were taken after the sample had been annealed to $\sim 450^\circ\text{C}$ [RHEED showed a faint (7×7) pattern]. Finally, the data in Fig. 3(c) were taken after an anneal to $\sim 650^\circ\text{C}$, during which the $(7 \times 7) \rightarrow (3 \times 1)$ transition was observed by RHEED. Several changes in the data are immediately apparent and can be quantified by fitting the data using Voigt line shapes. The solid lines in Fig. 3 are the results of these fits; the spectrum in Fig. 3(a) was fitted with a single spin-orbit doublet. Two doublets were used to fit the spectra in Figs. 3(b) and 3(c). The relevant fitting parameters are given in Table I. We also measured the $\text{F } 1s$ spectra, which were fitted by a single Voigt line shape with a variable Lorentzian width. The integrated intensities and widths, obtained from these fits, are shown as a function of temperature in Fig. 4.

Interpretation of photoemission spectra can be complicated by a lack of independent structural information. In this paper we use TEM images to aid our interpretation of the RHEED, x-ray, and photoemission results. All images are taken under standard two-beam conditions with the diffraction vector \mathbf{g} set slightly positive of the Bragg angle and with the incident beam direction a few degrees away from $[111]$. Figure 5(a) is a bright-field TEM image taken from a $\text{CaF}_2/\text{Si}(111)$ sample where CaF_2 was deposited at $T = 550^\circ\text{C}$ [RHEED showed a (1×1) pattern]. We assume that the regions with bright/dark edges are

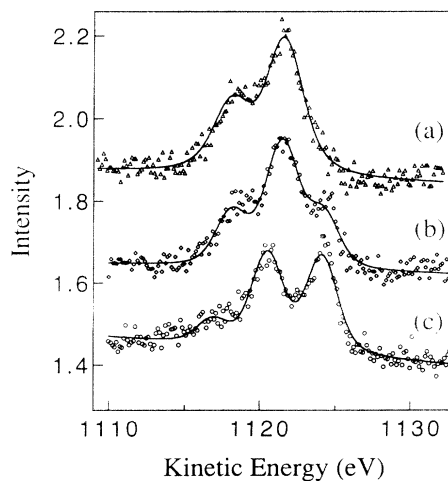


FIG. 3. $\text{Ca } 2p$ core-level XPS data taken from submonolayer coverages of CaF_2 on $\text{Si}(111)$ at (a) room temperature [RHEED showed a faint (7×7) pattern], (b) after the sample had been annealed to $T \sim 400^\circ\text{C}$ [RHEED still showed a faint (7×7) pattern], and (c) after the sample had been annealed to $T \sim 600^\circ\text{C}$ [RHEED showed a strong (3×1) pattern]. The data are displaced for clarity and the solid lines are Voigt line shape fits to the data in (a) with a single spin-orbit doublet and in (b) and (c) with two doublets. The fit parameters are listed in Table I.

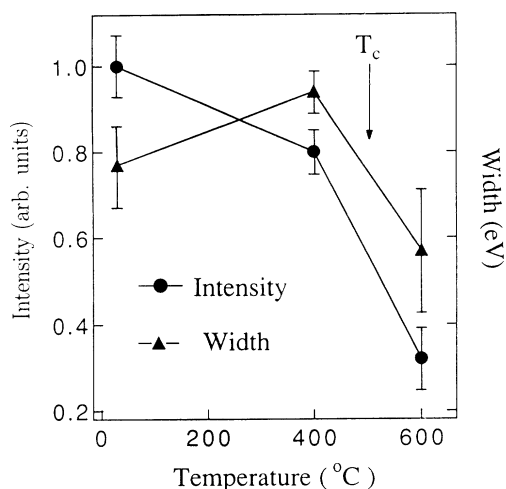


FIG. 4. Fit parameters to the F 1s core-level XPS data from the same sample described in Fig. 3 and at the same stages of the experiment. The integrated intensity is normalized to be 1 for the room-temperature result.

CaF₂ islands because the total coverage of these regions increases if more CaF₂ is deposited. The height of the islands cannot be directly determined from the TEM image, but was measured as ~ 4 CaF₂ triple layers thick by x-ray diffraction in a sample where the islands covered approximately 90% of the surface.⁷ The region in between the islands in Fig. 5(a) is not bare Si, since a (7×7) RHEED pattern was not observed and no (7×7) was visible in transmission electron diffraction (TED). Published MEIS, XPS, XSW, and STM work indicates the presence of CaF-Si(111) at submonolayer coverages.²⁻⁶ This suggests that the region in between the CaF₂ islands is a composite CaF-Si(111) layer.⁷ Figure 6(a) is a dark-field TEM image taken from a CaF₂/Si(111) sample where CaF₂ was deposited at $T=450^\circ\text{C}$ [RHEED and TED showed a weak (7×7) pattern].¹⁸ The small ($\sim 500\text{-\AA}$ -diam) regions bordered by bright and dark lines are CaF₂ islands. These islands appear to lie along $\frac{1}{3}[111]$ steps on the substrate. The weakened (7×7) RHEED pattern indicates that, at lower temperatures, CaF₂ islands grow directly onto the Si(111)- 7×7 surface, without a CaF-Si(111) wetting layer.

The TEM, x-ray scattering, and photoemission results enable a detailed description of the temperature dependence of CaF₂/Si(111) interface formation: At room tem-

TABLE I. Parameters to the fits to the XPS data in Fig. 3. The widths were fixed in fitting the spectra, which consists of a spin-orbit doublet (separated by 3.5 eV and with an intensity ratio 1:2) in (a) and two doublets in (b) and (c).

	I_1	I_2	I_{total}	Peak separation (eV)
(a)	3476	0	3476	
(b)	2511	1309	3820	2.6 ± 0.3
(c)	1240	2340	3580	3.9 ± 0.4

perature there is a weak interaction between the Si surface and the arriving CaF₂ molecules. The $(\frac{3}{7}, 0)$ superlattice Bragg reflection, specific to the Si- (7×7) reconstruction, is unchanged after deposition. The photoemission spectra show a single Ca 2p doublet, with a width consistent with Ca in a bulklike environment, and a broad F 1s line shape, possibly due to inhomogeneous broadening associated with fluorine disorder.¹⁹ The photoemission spectra change dramatically after the sample is annealed to $\sim 450^\circ\text{C}$, which is below the $(7 \times 7) \rightarrow (3 \times 1)$ transition temperature, but at a temperature where $\sim 50\%$ of the (7×7) was lifted in the x-ray

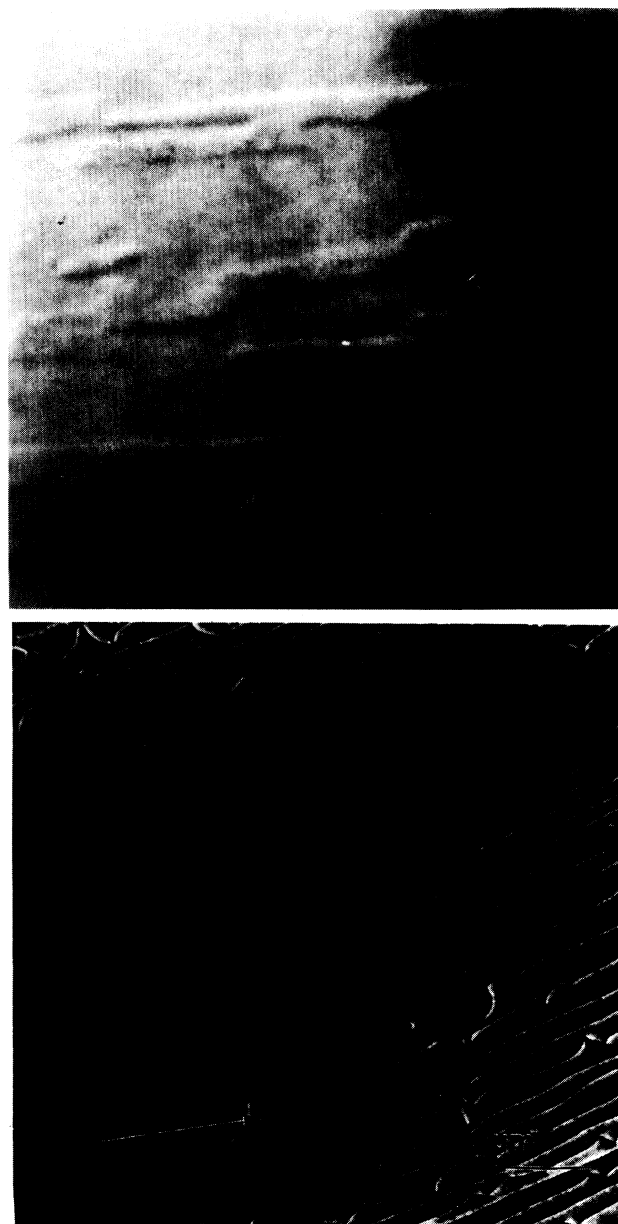


FIG. 5. TEM images taken from CaF₂/Si(111) samples. (a) Bright-field image after 8 sec of CaF₂ deposition at $T=550^\circ\text{C}$. (b) Dark-field image after 100 sec of CaF₂ deposition at $T=700^\circ\text{C}$. The appropriate $\langle 220 \rangle$ diffraction vectors are marked.

experiment. The Ca $2p$ spectrum now shows the presence of two doublets, separated by ~ 2.6 eV. This splitting is consistent with the separation between bulk and interface components observed in previous measurements of thin CaF_2 layers on Si(111).^{2,3} The peak at lower binding energy has been attributed to Ca-Si bonds at the interface. The decrease in the integrated intensity of the F $1s$ peak indicates that some dissociation and F desorption has occurred in the reaction of the Si-(7×7) surface. As the sample is heated to $\sim 650^\circ\text{C}$ the surface undergoes a

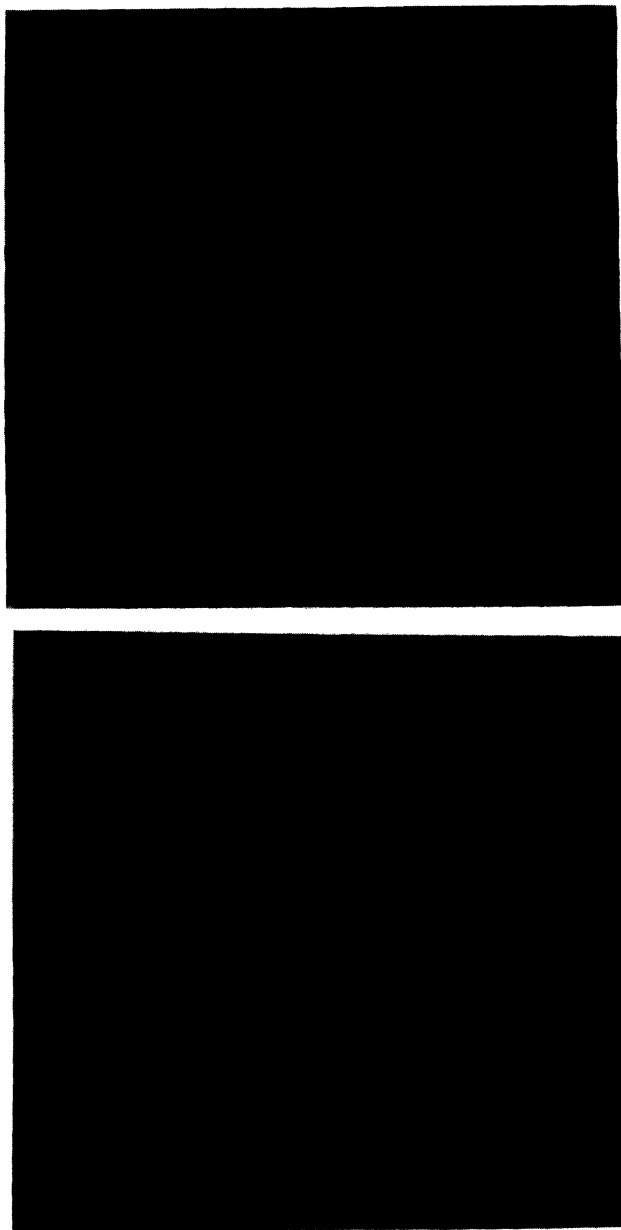


FIG. 6. Dark-field TEM images taken from $\text{CaF}_2/\text{Si}(111)$ samples grown at $T=450^\circ\text{C}$ (a) after 5 sec of CaF_2 deposition and (b) after 100 sec of CaF_2 deposition. The appropriate $\langle 220 \rangle$ diffraction vectors are marked.

(7×7) \rightarrow (3×1) transition and this overlayer wets the substrate. This is evidenced by the exchange of intensity between the $(\frac{2}{3}, 0)$ and $(\frac{1}{3}, 0)$ surface Bragg reflections shown in Fig. 2. The F $1s$ XPS peak sharpens and its integrated intensity drops by $\sim 50\%$. This is consistent with previous measurements of samples prepared at high temperatures ($T > 550^\circ\text{C}$) in which the CaF_2 molecule dissociates to give CaF at the interface and F in a single surface site. We cannot rule out the possibility that (3×1) and (1×1) phases coexist in the wetting layer and these two phases may have different Ca-F ratios. The correlation length of the (3×1) phase indicates that the reconstruction is very well ordered and covers areas of the surface with a domain size equivalent to that of the original Si-(7×7) reconstruction. This implies that the CaF_2 (or CaF) is remarkably mobile on the surface in changing from the island structure [in Fig. 6(a)] to the (3×1) phase. The Ca $2p$ XPS spectrum, above the transition temperature, still shows the presence of two doublets but now separated by ~ 4 eV and with an intensity ratio of $\sim 1:2$ (the most intense peak at lower binding energy). We suggest that this splitting is partially caused by the presence of two distinct Ca environments in the (3×1) reconstructed surface. The (3×1) phase can accommodate a range of coverage, which explains why it is the most commonly observed submonolayer reconstruction in this system.²⁰ Heating of the (3×1) phase to temperatures higher than 650°C can cause further depletion of F and a change in the intensity ratio of the two Ca $2p$ components. A detailed x-ray-diffraction study of the (3×1) surface is the subject of work in progress.²¹

Below the (7×7) \rightarrow (3×1) transition temperature the initial growth mode is Volmer-Weber, with CaF_2 islands



FIG. 7. Dark-field TEM image taken from a $\text{CaF}_2/\text{Si}(111)$ sample after 100 sec of deposition at room temperature. The inset is the $[111]$ transmission-electron-diffraction pattern from the same sample, taken at 200 keV. The pattern shows rings associated with the polycrystalline CaF_2 .

growing directly on the Si surface. Above the transition temperature the initial growth mode is Stranski-Krastanow with CaF_2 islands forming on the CaF wetting layer. Despite these different growth mechanisms and submonolayer structures, a pseudomorphic CaF_2 film results in both cases, and subsequent growth is layer by layer. Figures 5(b) and 6(b) show dark-field TEM images taken after 100 sec of CaF_2 deposition at substrate temperatures of 450°C and 700°C, respectively. An array of parallel line defects is visible and show contrast consistent with a displacement along $[11\bar{2}]$. Such line defects are anticipated at $\frac{1}{3}[111]$ steps on the Si substrate, as a consequence of differences between the symmetry operators of Si (space group $Fm\bar{3}m$) and the CaF_2 layer [space group $Fd\bar{3}m$ and rotated 180° about the (111) surface normal].²² The line defects in Fig. 5(b) show the same contrast as those in Fig. 6(b).

We have observed three temperature regimes in which pseudomorphic growth does not occur; growth at $T \leq 300^\circ\text{C}$, where there is no strong interface reaction, results in severe islanding. This is illustrated in Fig. 7, which is a dark-field TEM image taken after CaF_2 deposition at $T \sim 200^\circ\text{C}$. The inset to Fig. 7 is a TED pattern from the same sample showing the presence of polycrystalline rings. Islanding also results when the high- and low-temperature growth mechanisms coexist (at $T \sim 500^\circ\text{C}$). Submonolayer coverages in this case show islands on two different length scales, with large islands spanning some terraces [as in Fig. 5(a)] and much smaller islands on others [as in Fig. 6(a)]. Finally, growth at very high temperatures ($T > 800^\circ\text{C}$) can also result in islanding. This is presumably due to significant reevaporation of CaF_2 from the surface during growth. We should also note that changing the CaF_2 growth rate can bias the kinetics in favor of islanding on the CaF wetting layer and this has been described elsewhere.^{7,8}

IV. INTERFACE AND THIN-FILM STRUCTURE

The lattice mismatch between Si and CaF_2 varies from 0.6% at room temperature to $\sim 2.4\%$ at 700°C. The critical thickness for pseudomorphic films grown isothermally at 700°C is ~ 12 CaF_2 triple layers.^{12,23} However, the growth mechanisms described above, in which CaF_2 islands coalesce at a thickness of approximately four triple layers, suggest that a "template" method can be employed.^{7,11,24} Thick, unrelaxed CaF_2 films can be grown by depositing 6–7 layers at the desired temperature for interface formation and then cooling the sample to room temperature for subsequent growth. This method has been successful in achieving pseudomorphic growth up to a thickness of ~ 90 CaF_2 triple layers ($\sim 280 \text{ \AA}$). The samples described in the remaining sections of this paper were prepared by this template method in order to remove the effects of epilayer relaxation from the structural analysis.

Figure 8 is a HRTEM image taken along Si $[1\bar{1}0]$ from a nine triple-layer-thick $\text{CaF}_2/\text{Si}(111)$ film grown at 720°C. The 0.31-nm spacing of the $[111]$ and $[1\bar{1}\bar{1}]$ planes of the CaF_2 and Si are clearly resolved in this image. The abruptness of the $\text{CaF}_2/\text{Si}(111)$ interface and the twin orientation of the CaF_2 are readily apparent. This is consistent with diffraction contrast images taken from plan view samples which show no visible defects other than evenly spaced line defects with $\frac{1}{6}[11\bar{2}]$ character. In agreement with the experience of previous authors,^{9,25} we found it impossible to take a focal series of images, since the CaF_2 region of interest became amorphous after less than 1 min under the electron beam. The severity of the radiation damage inhibits the use of HRTEM as a tool to investigate the atomic structure of the $\text{CaF}_2/\text{Si}(111)$ interface.

Recently a technique has emerged which employs an

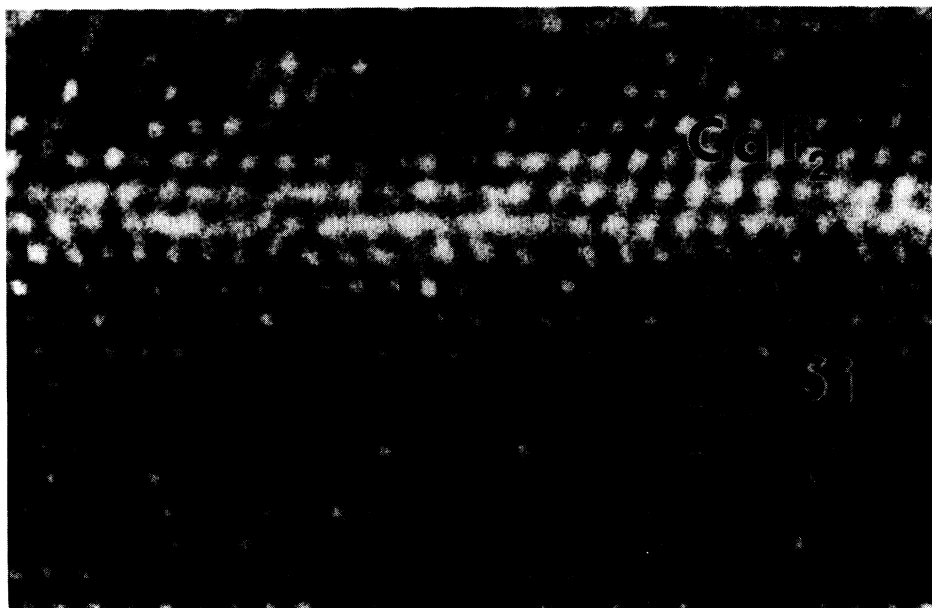


FIG. 8. High-resolution TEM image of the $\text{CaF}_2/\text{Si}(111)$ interface along the Si $[1\bar{1}0]$ direction, in a sample grown at $T = 720^\circ\text{C}$ and determined to be approximately nine CaF_2 triple layers ($\sim 30 \text{ \AA}$) thick. The point to point resolution is approximately 0.24 nm. The twin orientation (*B*-type stacking) of the CaF_2 film is readily apparent.

understanding of the x-ray “crystal truncation rod” (CTR), i.e., the x-ray scattering along the surface normal in reciprocal space through bulk Bragg reflections.²⁶ Figure 9(a) is a CTR measured through the Si(111) Bragg reflection along the (111) surface normal and extending over the range (0.9 0.9 0.9)–(1.1 1.1 1.1). The film was grown by the template method with initial deposition at $T=700^\circ\text{C}$. Each point corresponds to a background subtracted integrated intensity obtained by rocking scans, perpendicular to the CTR. The data points have been corrected for the variation in the active sample area and the Lorentz factor.²⁷ No data were collected close to the Bragg reflection, which would be approximately 1 on the intensity scale shown. Following the work of Robinson, Tung, and Feidenhansl²⁸ and our previous paper,¹² we fit the data to a model with four parameters: N , the number of CaF_2 layers; c , the out-of-plane lattice parameter of the CaF_2 film; d , the interfacial separation, which is the distance from the midpoint of the top Si bilayer to the first Ca atom in the film; and an overall scale factor which multiplies the calculated intensity and accounts for the fact that the measurements are not normalized to the incident x-ray beam intensity. The best fit shown by the solid line in Fig. 9(a) gives $N=29$, $c=3.168\pm 0.004 \text{ \AA}$, and $d=2.8\pm 0.1 \text{ \AA}$. With the CaF_2 epilayer distorted in plane to match the Si lattice constant, as shown by the lack of moiré fringes in the TEM image [e.g., Fig. 5(b)], the perpendicular lattice constant increases to accommodate the strain and can be calculated from the elastic constants using Poisson’s ratio.²⁹ The calculated value is in good agreement with the measured value. The interface separation d is consistent with the ion scattering mea-

surements of Tromp and Reuter ($d=2.67 \text{ \AA}$) (Ref. 4) and the XSW measurements by Zegenhagen and Patel ($d=2.73 \text{ \AA}$),⁶ which were both performed on 1-ML-thick films (it was concluded from these and other measurements that the high-temperature interface was deficient in F and so the interface F layer was removed in our scattering model).

Figure 9(b) shows another CTR from a sample initially grown at $T=450^\circ\text{C}$. The parameters to the fit are $N=42$, $c=3.168\pm 0.004 \text{ \AA}$, and $d=3.3\pm 0.2 \text{ \AA}$. The CaF_2 lattice parameter is the same for both samples as the measurements were performed at room temperature and neither film had relaxed. The interfacial separation d , however, is different and causes the change in asymmetry around the Si Bragg reflection. The relatively poor quality of the fit to the data in Fig. 9(b) indicates that the model is inadequate and suggests that there may be a mixture of bonding sites at the interface. This is supported by previous XPS results in which a component in the Si $2p$ spectrum, shifted by $\sim 0.8 \text{ eV}$ to a higher binding energy than the bulk Si $2p$ component, was observed at a deposition temperature $T=500^\circ\text{C}$ and attributed to the presence of Si-F bonds at the interface.² An increase in the interface separation as the deposition temperature was decreased was also observed by XSW.⁶ It is remarkable that at low temperatures a pseudomorphic CaF_2 film is formed, given the apparent mixture of bonding schemes at the interface. This may be linked to the recent observation that Si adatoms are incorporated in the initial CaF layer at low growth temperatures.³⁰

The CTR technique attains sensitivity to single monolayers if the measurement is performed over very large ranges of momentum transfer, well away from the bulk Bragg reflections.³¹ For a thin-film system, the scattered amplitude at any point along a truncation rod is the sum of the contributions from the substrate and the film, and it is the interference between these components that provides the sensitivity to the detailed atomic structure. As all layers that are commensurate with the substrate contribute to the scattering, the interpretation can be complicated due to the influence of atomic scale roughness, such as vacancies or steps. It is for this reason that there have been few studies of epitaxial films, which often contain a variety of structural defects.³² The quality of the TEM images in Figs. 5(b) and 6(b) suggests that $\text{CaF}_2/\text{Si}(111)$ is a prototypical system for a detailed CTR study.

Within the kinematical approximation, the scattering amplitude from an arbitrary unit cell is given by

$$A(\mathbf{Q}) = \sum_j f_j(\mathbf{Q}) e^{i\mathbf{Q}\cdot\mathbf{r}_j}, \quad (1)$$

where there are j atoms in the unit cell at positions \mathbf{r}_j and $f_j(\mathbf{Q})$ is the atomic form factor.³³ The total scattered amplitude is obtained by summing over the unit cells in the structure. For a Si(111) crystal we use the standard LEED notation for the hexagonal unit cell. This is related to the cubic unit cell by the transforms

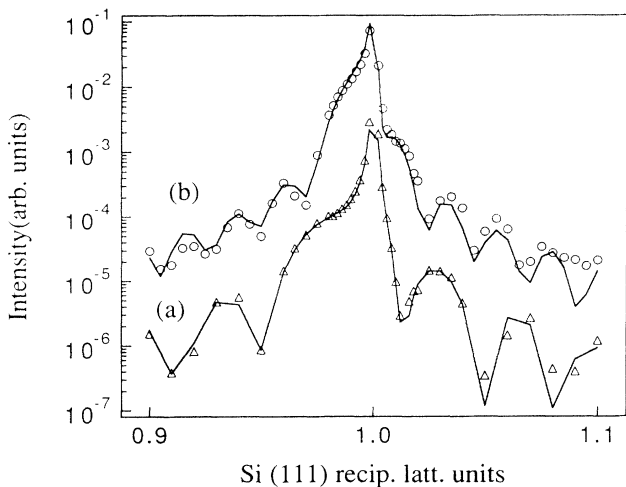


FIG. 9. Integrated intensity of the x-ray diffraction along the surface normal direction (specular CTR) through the Si(111) Bragg reflection, from two samples grown by the template method with (a) initial deposition at $T=700^\circ\text{C}$ and (b) initial deposition at $T=450^\circ\text{C}$. For (a) the Si Bragg peak would be approximately 1 on the intensity scale shown. The data set (b) is displaced for clarity. Solid lines are fits to the data according to a simple kinematical scattering model with four independent structural parameters.

$$\begin{aligned}
 (100)_h &= \frac{1}{3}(22\bar{4})_{\text{cub}}, \\
 (010)_h &= \frac{1}{3}(\bar{2}4\bar{2})_{\text{cub}}, \\
 (001)_h &= \frac{1}{3}(111)_{\text{cub}}.
 \end{aligned}
 \tag{2}$$

In this notation the Miller indices h and k represent the in-plane momentum transfer and l is perpendicular to the surface. For the Si substrate the scattering is given by

$$A_{\text{Si}}(h, k, l) = f_{\text{Si}}(h, k, l) \sum_{n=-\infty}^0 \{1 + \exp(2\pi i[2h/3 + k/3 + l/12])\} \exp(in\mathbf{r}) \tag{3}$$

$$= f_{\text{Si}}(h, k, l) \frac{\{1 + \exp(2\pi i[2h/3 + k/3 + l/12])\}}{1 - \exp(-2\pi i[2h/3 + k/3 + l/3])}. \tag{4}$$

The CaF_2 film has a three-atom basis with a unit cell defined by the vectors

$$\begin{aligned}
 \mathbf{r}_1 &= 0 \quad (\text{Ca atom}), \\
 \mathbf{r}_2 &= \frac{1}{3}(2\mathbf{a}_1 + \mathbf{a}_2) - \mathbf{a}_3/12, \\
 \mathbf{r}_3 &= -\frac{1}{3}(2\mathbf{a}_1 + \mathbf{a}_2) + \mathbf{a}_3/12 \quad (\text{F atoms}).
 \end{aligned}$$

The shift between adjacent CaF_2 triple layers is given by $\mathbf{r} = -\frac{2}{3}\mathbf{a}_1 - \frac{1}{3}\mathbf{a}_2 + \frac{1}{3}\mathbf{a}_3$, where the negative sign in the first two indices accounts for the B -type stacking in the CaF_2 film, i.e., a 180° rotation in the direction of the stacking with relation to the Si bilayers. For a N layer CaF_2 film the summation gives a scattering factor

$$\begin{aligned}
 A_{\text{CaF}_2} &= \{f_{\text{Ca}} + 2f_{\text{F}} \cos[2\pi(2h/3 + k/3 - l/12)]\} \\
 &\times \frac{1 - \exp\{2\pi iN[-2h/3 - k/3 + (\frac{1}{3} + \Delta)l]\}}{1 - \exp\{2\pi i[-2h/3 - k/3 + (\frac{1}{3} + \Delta)l]\}}.
 \end{aligned}
 \tag{5}$$

Δ accounts for the difference of the CaF_2 and Si lattice parameters in the out-of-plane direction and it is assumed that there is lattice matching in plane. The total scattered amplitude is the sum of the scattering from the film and the substrate, with an appropriate phase factor multiplying A_{CaF_2} , given by

$$\psi_{h,k,l} = \exp[2\pi i(xh + yk + zl)], \tag{6}$$

where $x\mathbf{a}_1 + y\mathbf{a}_2 + z\mathbf{a}_3$ is the shift from the Si bilayer to the first Ca atom. The scattered intensity is

$$I_{h,k,l} \propto |A_{\text{Si}}(h, k, l) + \psi_{h,k,l} A_{\text{CaF}_2}(h, k, l)|^2. \tag{7}$$

For the $(10l)$ rod there is divergence at the Si Bragg reflections at $l = -5, 1, 4$ but not at $l = -2$, which is systematically absent for the diamond structure.

Figures 10(a) and 10(b) show the measured scattering along the $(10l)$ rod for an uncapped film grown by the template method with initial deposition at 700°C . The measurement was performed on beam line 7-2 at SSRL, using the standard $\omega=0$ four-circle configuration of the diffractometer.³⁵ Each point along the rod corresponds

the summation over the Si bilayers,³⁴ each bilayer containing two atoms at positions $\mathbf{r}_1=0$ and $\mathbf{r}_2=\frac{2}{3}\mathbf{a}_1 + \frac{1}{3}\mathbf{a}_2 + \frac{1}{12}\mathbf{a}_3$, where the vectors \mathbf{a}_i correspond to real-space vectors defined by the reciprocal-space lattice in Eq. (2). Each bilayer is shifted by $\mathbf{r}=\frac{2}{3}\mathbf{a}_1 + \frac{1}{3}\mathbf{a}_2 + \frac{1}{3}\mathbf{a}_3$ with respect to the neighboring bilayer below. Neglecting absorption, the scattering from the semi-infinite Si substrate is

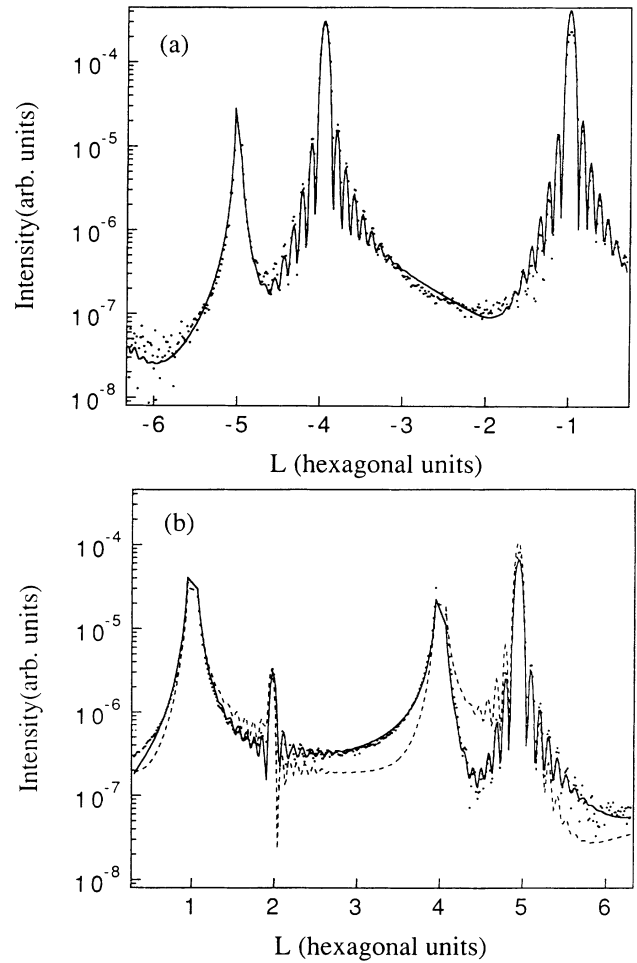


FIG. 10. The extended CTR scattering from a 28 CaF_2 triple-layer-thick sample grown by the template method. (a) The scattering along $(\bar{1}0l)$ defined using the hexagonal unit cell in Eq. (2). The data are mapped onto $(10\bar{l})$ according to Friedel's inversion rule. (b) The scattering along $(10l)$. The Si Bragg peaks at $l = -5, 1, 4$ are approximately 1 on the intensity scale shown. The solid line is a fit to the data according to the model described in the text and the parameters in Table II. The dashed line in (b) is a calculation with the first Ca atom at the interface in an H_3 bonding site.

to a background subtracted integrated intensity obtained in a ϕ scan, which is a rotation about the sample surface normal. At low l values, where the resolution is dominated by the vertical divergence of the incident beam, the ϕ scans exhibited two narrow peaks due to the regular step distribution on the surface.³⁶ At higher l values the resolution is defined by a convolution of the horizontal divergence of the incident beam and the angular acceptance of the detector slits and the ϕ scans showed a single broad peak. The resolution along l was always sufficient to resolve the oscillation fringes seen in Fig. 10 without any broadening or dampening effects. This was checked by changing the slit sizes and repeating some of the data collection. There are a total of ~ 1000 points in Figs. 10(a) and 10(b). As it is only possible to measure at positive l values, the data in Fig. 10(a) is actually a measure of the $(\bar{1}0l)$ rod, which is equivalent to $(10\bar{l})$ according to Friedel's inversion rule. It should be noted that the Si Bragg reflections are ~ 1 on the intensity scale shown and so the use of synchrotron radiation is essential for this measurement.

To extract structural information from the CTR data it is necessary to develop a scattering model based on the equations given above. A number of changes to the simplified model are required in order to obtain a good fit to the data and we will discuss these in turn. First of all, the data must be corrected for instrumental resolution effects, which we include in the calculation of the CTR profile. The resolution function appropriate to CTR data collected in this way has been described in detail by Toney and Wiesler.³⁷ The second factor that we take into consideration is that our structural model must be consistent with previous measurements of the $\text{CaF}_2/\text{Si}(111)$ interface. It has been shown by a number of authors that, for deposition at high temperatures, the CaF_2 molecule dissociates to give CaF at the interface. It is simple to remove the first F layer in the scattering model. The interface separation we obtain from the specular CTR scattering [Fig. 9(a)] implies that there are two possible sites for the first Ca atom if sensible Ca-Si bond lengths are to be retained. These are the H_3 site, above the fourth layer Si atoms, and the T_4 site, above second layer Si atoms. The locations of these sites with relation to the bulk Si lattice are shown in Fig. 11. They are related by a translation vector $\frac{1}{3}(\mathbf{a}_1 - \mathbf{a}_2)$ and so the change from H_3 to T_4 has a dramatic effect on the $(10l)$ rod, as it alters the phase of A_{CaF_2} with respect to A_{Si} . The final alteration is to take into account the effects of roughness. The simplest example is a variation in the number of CaF_2 layers, i.e., a discrete thickness variation across the illuminated area of the surface. We include this by giving the layer thickness a discrete Gaussian distribution about a mean value N and summing this distribution in Eq. (7). This assumes that steps on the CaF_2 surface have a large in-plane correlation length. In addition to the thickness distribution, each atomic layer in the scattering model is given a surface-normal root-mean-square displacement amplitude σ_i by multiplying the atomic form factors f_i in Eqs. (4) and (5) by a static Debye-Waller factor $\exp(-Q_z^2 \sigma_i^2)$. Q_z is the surface normal momentum

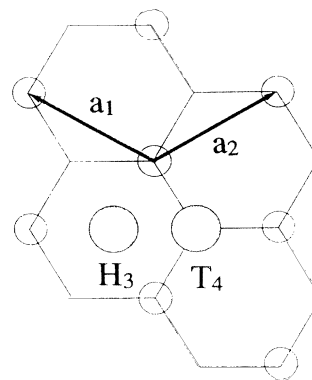


FIG. 11. Top view of the Si surface unit cell. The two possible adsorption sites T_4 and H_3 for the Ca atom in the CaF layer at the interface are shown by the shaded atoms. The basis vectors of the hexagonal unit cell are indicated.

transfer, proportional to l .

Using a least-squares minimization routine the best fit to the data is shown by the solid lines in Figs. 10(a) and 10(b), according to the structural parameters in Table II. A number of structural models were tested in which the strain in the CaF_2 epilayer and the roughness at the Si/CaF_2 interface and CaF_2 surface were altered. As the measurement is a nonspecular CTR, layers that contribute to the scattering must be ordered in the surface plane and commensurate with the Si substrate. Models in which both the strain and the atomic scale roughness were given distributions, with exponential decay away from the interfaces governed by independent correlation lengths,³⁸ were tried, but did not improve the fit to the data. Including a stacking fault in the topmost Si bilayer has a dramatic effect on the calculated profile³⁹ and is not consistent with the data.

The structural information we obtain from this measurement is as follows.

(i) The solid line and dashed line in Fig. 10(b) are calculations with the first Ca atom in a T_4 site and an H_3 site, respectively. Clearly the data support a T_4 bonding site. If the population of T_4 and H_3 sites is allowed to vary, the best fit is for 100% T_4 . This disagrees with previous XSW and x-ray-diffraction measurements, which suggested an equal population of T_4 and H_3 sites resulting in a domain structure in the CaF_2 film.¹⁰ We see no evidence of such a domain structure and attribute the previous results to nonuniform growth. The XSW measurements⁶ were performed on submonolayer coverages where it is possible that a mixture of bonding sites is present. Our results are consistent with the MEIS studies of Tromp and Reuter,¹⁴ which were performed on structures exhibiting a (1×1) LEED pattern. The CTR measurement is extremely sensitive to the choice of bonding site since it directly determines the interference between the scattering from the CaF_2 overlayers and the substrate.

(ii) The results show that the CaF_2 film is lattice matched in-plane to the Si substrate. This distortion re-

TABLE II. Summary of the parameters in the structural model used to calculate the solid line in Fig. 10. The errors in the fitted parameters are difficult to evaluate from a χ^2 analysis, due to the large number of data points, but it is expected that the quoted figures are significant.

Si surface	Top atom relaxation of -0.1 \AA (into surface)
CaF ₂ /Si interface	Ca in T_4 bonding site Interface spacing (middle of Si bilayer to Ca atom) $d = 2.74 \text{ \AA}$ $d_{\text{Ca1}} - d_{\text{Ca2}}$ (CaF layer to first CaF ₂ layer spacing) = 3.184 \AA
CaF ₂ film	Number of layers $N = 28$ Gaussian width $\sigma_N = 1.40$ CaF ₂ (111) lattice parameter $c = 3.174 \text{ \AA}$ ($c_{\text{Si}} = 3.1356 \text{ \AA}$)
Roughness parameters	$\sigma_{\text{Ca}} = 0.06 \text{ \AA}$, $\sigma_{\text{F}} = 0.26 \text{ \AA}$, $\sigma_{\text{Si}} = 0.15 \text{ \AA}$
Surface roughness	No surface F layer $\sigma_0 (\text{Ca}) = 0.87 \text{ \AA}$

sults in an expansion in the out-of-plane CaF₂ lattice constant. There is no evidence to support a strain variation in the surface normal direction in the CaF₂ film or at the surface of the Si substrate. It should be noted that the TEM image in Fig. 5(b) indicates that there is a strain field around the misfit dislocations. However, this is a second-order effect on the CTR, due to the small fraction of material involved.

(iii) Although the CTR measurement is not sensitive to noncrystalline material, the results do give some insight into the structure at the CaF₂ surface. The best fit to the data includes a missing (or completely disordered) F layer at the surface. The disorder is propagated to the first Ca layer, manifested in an increased σ value. This surface remains stable over long-time periods, indicating that the reaction is localized at the surface.

(iv) The values σ_i are independent of the thermal Debye-Waller factors which have been explicitly included in the calculation. The effect of bond charge distribution in Si, where each atom contributes one electron to the covalent bond,⁴⁰ has not been included and may account for the nonzero value of σ_{Si} .

(v) The layer thickness is described by a discrete Gaussian distribution centered about $N = 28$. For the calculated σ_N in Table II this implies that the thickness variation is over five CaF₂ triple layers, i.e., $\sim 21\% N = 26, 30$; $\sim 46\% N = 27, 29$; and $\sim 33\% N = 28$. The x-ray measurement typically samples a surface area of $\sim 2 \text{ mm}^2$.

Real-space structural information to support the CTR model was obtained by performing dark-field TEM measurements. A rotation of 180° about $[111]$ is not a symmetry operation for a cubic lattice. Scattering from the CaF₂ layer can be separated from scattering from the Si substrate since the CaF₂ $[11\bar{1}]$ is coincident with the disallowed, weak Si $[\frac{5}{3}\frac{1}{3}\frac{1}{3}]$ reflection (the notation used here is for the conventional bulk unit cell). Dark-field images formed using CaF₂ $[11\bar{1}]$ are therefore dominated by diffraction contrast originating in the CaF₂ layer only. Figure 12 shows a $[11\bar{1}]$ dark-field image taken from a

CaF₂ layer grown at 700°C . The thickness of the layer was 4–5 triple layers, as determined by the ratio of the interface to bulk components in the Ca $2p$ XPS signal. The CaF₂ layer is thin enough to make a kinematical scattering approximation valid and yet thick enough to allow the small contribution from the Si to be ignored. Image brightness can therefore be interpreted as being



FIG. 12. TEM micrograph, imaged with CaF₂ $[11\bar{1}]$, from a CaF₂/Si(111) film deposited at a substrate temperature $T = 770^\circ\text{C}$ to a thickness of approximately five CaF₂ triple layers. The diffraction vectors are marked and the scale bar is $0.5 \mu\text{m}$ long. The incident beam direction is close to $[123]$. Changes in thickness of one CaF₂ triple layer ($\frac{1}{3}[111]$) appear as a change in brightness of the image. $\frac{1}{3}[111]$ steps at the interface, which are correlated with the array of line defects seen in Fig. 5(b), are visible, as are the $\frac{1}{3}[111]$ steps at the CaF₂ surface.

proportional to the CaF_2 thickness. Two sets of intersecting steps, one straight and one slightly faceted, are clearly visible in Fig. 12. Line defects at the straighter steps come into contrast as either dark or light lines if the sample is tilted away from the exact CaF_2 $[11\bar{1}]$ Bragg condition. From symmetry considerations it is known that line defects with $\frac{1}{6}[11\bar{2}]$ character are introduced at $\frac{1}{3}[111]$ steps on the Si surface (see above). The straight steps therefore lie at the CaF_2/Si interface and the more faceted set of steps lie at the top surface of the CaF_2 . There are only three contrast levels in Fig. 12 (apart from completely black regions, which are holes). It can therefore be inferred that the thickness of the film varies over three CaF_2 triple layers and that the steps on the top and bottom of the film are one triple layer high. Dark-field images from CaF_2 layers of different thicknesses indicate the same morphology. In films thicker than ~ 20 triple layers the dark-field contrast is lost under the diffuse background⁴¹ and interpretation of the images is complicated by multiple scattering. To exclude as much of the diffuse background as possible an extremely small objective aperture is used (1 mrad diam). Dark-field images showing qualitatively similar contrast to Fig. 12 have been taken from Au,⁴² Si,⁴³ and MgO.⁴⁴ To our knowledge the present observations are the first to show the distribution of atomic steps at the top and bottom surfaces of an epitaxial film. Further discussion of this dark-field contrast will be published elsewhere.⁴⁵ In conclusion, $\text{CaF}_2[11\bar{1}]$ dark-field images show wide terraces on the CaF_2 surface separated by triple layer high steps, which have a tendency to form facets along $\langle 110 \rangle$. This supports the CTR model of film height distribution.

V. INTERFACE STRUCTURAL TRANSITION

In a recent paper we presented measurements that indicated that the $\text{CaF}_2/\text{Si}(111)$ interface undergoes a structural transition.¹¹ On the basis of the available data set we concluded that the buildup of strain in the thin film was the driving force for this transition. After further study we find that this transition is considerably more complex and that strain is not the primary driving force. The transition may well explain some of the discrepancies between previous measurements of the $\text{CaF}_2/\text{Si}(111)$ interface structure and should be considered in future work on this system, particularly if comparisons between *in situ* (i.e., under UHV growth conditions) and *ex situ* experiments are to be made.

Figure 13 shows x-ray-diffraction measurements, taken with a rotating anode x-ray source as described in Sec. IV, over the range $l=0.95-1.05$ around the $\text{Si}(111)$ Bragg reflection. The sample was grown by the template method and, from the oscillation period in the x-ray data, is determined to be 27 CaF_2 triple layers thick. The three data sets in Fig. 13 were taken after ~ 2 days, 16 days, and 60 days for curves (a), (b), and (c), respectively. A dramatic change in the data is observed, most notably at $l \sim 1.02$, where the change in integrated intensity is greater than a factor of 10 between (a) and (c). The solid lines are fits to the data with the simple four-parameter

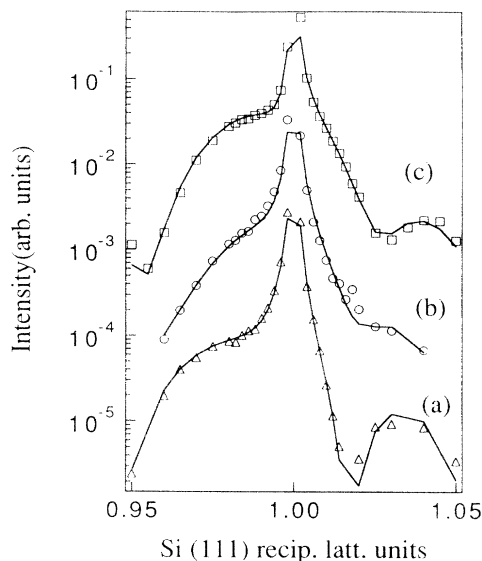


FIG. 13. Measurements of the specular CTR, similar to those in Fig. 9, for a sample grown by the template method with initial deposition at $T=700^\circ\text{C}$. The thickness is ~ 27 CaF_2 triple layers. The data were taken (a) 2 days, (b) 16 days, and (c) 60 days after the sample had been removed from the MBE vacuum chamber. The data are displaced for clarity and the solid lines are fits to the data with the simple four-parameter model. The only parameter that changes is the interface separation d .

model described previously. The fits all give a distortion of the out-of-plane CaF_2 lattice constant $c=3.17 \text{ \AA}$ and the same layer thickness (no height distribution is included in this model). The only parameter that changed is the interface separation d . In (a) $d=2.8 \text{ \AA}$, consistent with the measurements in Sec. IV. In (c) $d=4.5 \text{ \AA}$ and the fit in (b) is obtained by an incoherent sum of the scattering from $d=2.8$ and $d=4.5 \text{ \AA}$ interfaces. The value $d=4.5 \text{ \AA}$ is not a physically reasonable spacing between the substrate and epilayer and we assume that there is a layer in between the two lattices. Such a layer would not greatly influence the x-ray measurement as the technique is based on the interference of the scattering from the two "bulk" crystals (film and substrate).^{12,28} The results of Figs. 13(a) and 13(c) are consistent with the measurements described in our previous paper.¹¹ The transition probably occurs from one discrete interface structure to another, as the data in Fig. 13(b) are adequately modeled by a mixture of the initial and final interface separations. There is one important point to note; the measured line shapes in the x-ray measurement, obtained by scanning perpendicular to the rod of scattering, are unchanged throughout the experiment. Planview TEM images of the sample, such as Fig. 5(b), are also unchanged. This indicates that the interface transition is not a result of relaxation in the CaF_2 film.

We have examined some of the dynamics of the structural transition and it exhibits the following characteristics.

- (i) The time elapsed before the transition occurs is criti-

cally dependent on the thickness of the CaF_2 epilayer. We have never observed the $d=2.8 \text{ \AA}$ interface in a film where the thickness is less than 15 triple layers (the x-ray measurement takes approximately 4 h to perform after the sample has been removed from the vacuum). The time scale for thicker films varies from ~ 1 day to less than 1 month.

(ii) The transition appears to be independent of the thickness of the amorphous Si capping layer, which has been varied from 0 to 500 \AA .

(iii) All of the samples we have measured eventually undergo this transition and the new interface ($d=4.5 \text{ \AA}$) is stable for much longer time periods (greater than 1 year). The transition also occurs in films that are completely or partially relaxed.

(iv) The transition has also been observed by Raman scattering, where it is signified by the disappearance of a sharp interface peak at 448 cm^{-1} .⁴⁶

(v) The time scale depends on the doping of the Si substrate with a faster transition for *n*-type doped wafers (the carrier concentration in both the *n*-type and *p*-type wafers was measured as $\sim 1 \times 10^{16} \text{ cm}^{-3}$).

The new interface structure is more complicated than the as-grown structure. Figure 14(a) shows part of a [111] TED pattern, taken at 200 keV, from an 18 triple-layer-thick CaF_2 layer, and several weeks after the sample had been removed from the MBE vacuum chamber. The brightest peaks are reciprocal-lattice points which have a nonzero structure factor for bulk Si and CaF_2 . Weaker peaks at $\frac{1}{3}\langle 224 \rangle$ are disallowed for the bulk but allowed at a (111) interface/surface. The weakest features, in $\frac{1}{3}\langle 220 \rangle$ positions, are consistent with a $(\sqrt{3} \times \sqrt{3})R 30^\circ$ unit cell, indexed using the Si surface unit cell. This reconstruction must occur at the interface, as the $(\sqrt{3} \times \sqrt{3})R 30^\circ$ was not observed by RHEED from a sample which had been exposed to the atmosphere. We also searched for $(\sqrt{3} \times \sqrt{3})R 30^\circ$ superlattice reflections using grazing incidence x-ray scattering at SSRL. With the crystallographic alignment determined by several in-plane Si Bragg reflections, no intensity was observed at the superlattice positions defined by the $(\sqrt{3} \times \sqrt{3})R 30^\circ$ symmetry. Intensity was observed, however, at a position incommensurate with the $(\sqrt{3} \times \sqrt{3})R 30^\circ$ reciprocal-space lattice. Figure 14(b) shows a ϕ scan (rotation around the sample surface normal) centered at (0.27, 1.37) in the Si hexagonal cell notation defined in Eq. (2) [a commensurate $(\sqrt{3} \times \sqrt{3})R 30^\circ$ reflection would occur at $(\frac{1}{3}, \frac{4}{3})$]. The peak intensity in Fig. 14(b) is only 17 counts per second and illustrates the weakness of the scattering. The sharpness of the peak implies a large domain size and there is some evidence for oscillatory behavior in the tails of the scattering. Due to the low scattering factor and the sharpness of the peak, coupled with the fact that the peaks do not lie at symmetry positions, we were unable to find any other reflections.

At present we cannot identify a driving force for the interface transition. An obvious candidate would be a contamination effect, as a result of the interaction with the air. However, the transition is uninhibited by the presence of the Si capping layer, which provides an

effective barrier to most contaminants. The critical dependence of the reaction time on the thickness of the CaF_2 film implies that the transition is initiated at the surface and the time dependence governed by diffusion to the interface. This could be linked to the creation of F vacancies at the surface, which is implied by the structural model derived from the CTR measurements in Sec. IV.

The dominant defect in the alkali-earth fluorides is caused by Frenkel disorder, in which some of the negative fluoride ions move to interstitial lattice sites causing

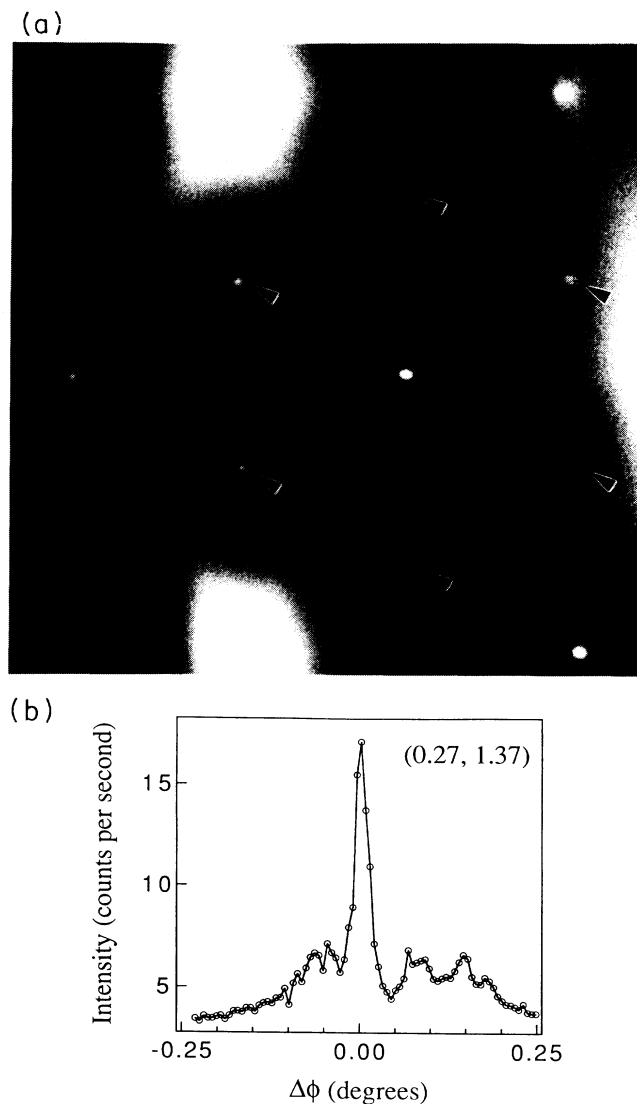


FIG. 14. (a) Part of a [111] transmission-electron-diffraction pattern from an 18 triple-layer-thick CaF_2 film. The features marked with arrows lie close to $\frac{1}{3}\langle 220 \rangle$ positions and can be attributed to a reconstructed layer at the $\text{CaF}_2/\text{Si}(111)$ interface, with a $(\sqrt{3} \times \sqrt{3})R 30^\circ$ symmetry, indexed using the Si unit cell. (b) A grazing incidence x-ray rocking scan at (0.27, 1.37, 0.05) in the reciprocal lattice notation defined in Eq. (2). For a commensurate $(\sqrt{3} \times \sqrt{3})R 30^\circ$ reconstruction there would be a peak at $(\frac{1}{3}, \frac{4}{3}, 0)$. The peak center is displaced away (a rotation of $\sim 1.9^\circ$) from the commensurate position. The solid line is a guide to the eye.

fluoride vacancies at regular lattice sites. In addition, fluoride films are susceptible to radiation damage which can create F-center defects.⁴⁷ A F center is created when a fluorine atom is removed from a lattice site and replaced by an electron.⁴⁸ Recently, Weiss, Wiemhöfer, and Göpel⁴⁹ calculated diffusion constants for fluorine interstitial ions and fluorine vacancies in CaF_2 and showed that fluorine vacancies are extremely mobile, even at room temperature. It is possible that defects, intrinsic to the ionic film or created at the surface, could diffuse to the interface and, at a threshold concentration, drive the transition to the observed $(\sqrt{3} \times \sqrt{3})R30^\circ$ structure. F centers are known to "migrate" with applied fields. This may explain the dependence on the Si doping level, as the different band bending potentials can modify the defect diffusion constants. The intrinsic defect concentration depends on the growth temperature of the CaF_2 film. However, a systematic study of these properties is difficult because the interface must be grown above the $(7 \times 7) \rightarrow (3 \times 1)$ transition temperature and the CaF_2 film must be thick enough to allow a measurement of the as-grown interface structure.

Clearly, the as-grown $\text{CaF}_2/\text{Si}(111)$ interface is a metastable phase which eventually transforms to a different structure. This is an obvious cause for the discrepancies between previous experiments which involved a variety of *in situ* and *ex situ* characterization techniques. An understanding of the interfacial structure and its metastability is important to the interpretation of other results; it is the atomic structure at the buried interface that determines the electronic properties. We plan to perform a quantitative TED structure factor analysis of the $(\sqrt{3} \times \sqrt{3})R30^\circ$ interface reconstruction. In combination with CTR measurements, similar to those in Fig. 10, we should be able to derive a structural model. We note that a $(\sqrt{3} \times \sqrt{3})R30^\circ$ reconstruction has also been observed at the $\text{CoSi}_2/\text{Si}(111)$ interface under certain growth conditions.⁵⁰ This is thought to involve a reordering of the surface Si atoms.

VI. CONCLUSIONS

In this paper we have described a comprehensive study of the early stages of interface formation, the temperature dependence of the growth modes, and the interface and thin film structure in $\text{CaF}_2/\text{Si}(111)$. The results have been obtained using a powerful combination of *in situ* and *ex situ* experimental techniques: core-level photoemission, RHEED, x-ray diffraction, and TEM.

At submonolayer coverages three distinct temperature regimes are observed; at room temperature there is little reaction between the arriving CaF_2 molecules and the $\text{Si}(111)-(7 \times 7)$ reconstructed surface. At slightly higher temperatures ($T=200-500^\circ\text{C}$), the (7×7) is removed, but no ordered submonolayer phases are observed and growth occurs as small islands. At $T \sim 500^\circ\text{C}$ the surface undergoes a transition to a (3×1) reconstruction which involves dissociation of the CaF_2 molecule to give a CaF wetting layer on the Si surface. Growth at temperatures above this transition occurs by islands, approximately four CaF_2 triple layers high, which are elongated along

the step terraces on the surface. At temperatures, above $T \sim 200^\circ\text{C}$, the islands eventually join up to form a continuous, pseudomorphic CaF_2 film.

We have studied the interface structure grown at high temperature ($T > 500^\circ\text{C}$) and low temperature ($200^\circ\text{C} > T > 500^\circ\text{C}$), by a combination of x-ray diffraction and TEM. The interface spacing d , which is the spacing between the Si and CaF_2 lattices and is directly measured in a CTR experiment, is larger at low growth temperatures and this is consistent with previous XPS measurements, which indicated incomplete dissociation of CaF_2 at the interface. The high-temperature interface was studied using synchrotron radiation to extend the CTR measurement and obtain sensitivity to the atomic-scale details of the CaF_2 surface and CaF_2/Si interface structure. The results are consistent with a single T_4 bonding site for the initial Ca atom in the CaF layer at the interface.

Finally, the as-grown CaF_2/Si interface is observed to undergo a structural transition, with a time dependence that is critically dependent on the thickness of the CaF_2 film. The transition appears to be initiated at the surface with the kinetics being governed by diffusion to the interface. The new structure involves an incommensurate $(\sqrt{3} \times \sqrt{3})R30^\circ$ interface reconstruction, which we are attempting to solve using a combination of quantitative TED and CTR analysis. It is hoped that a structural model of this interface will give some insight into the driving force for the transition. This transition is probably responsible for some of the discrepancies between previous measurements of the $\text{CaF}_2/\text{Si}(111)$ interface properties. It would be very interesting to correlate the different interface structures with the electronic properties of the interface.

ACKNOWLEDGMENTS

We would like to thank Peter Eng (University of Illinois), Oleh Karpenko (University of Michigan), and Alex Payne and Paul Fuoss (AT&T Bell Laboratories) for their contribution to the work performed at NSLS, Brookhaven. Beamline X16A is supported by AT&T Bell Laboratories. Research carried out at the National Synchrotron Light Source, Brookhaven National Laboratory, is supported by the U.S. Department of Energy, Division of Materials Sciences and Department of Chemical Sciences (DOE Contract No. AC02-76CH00016). We acknowledge the hospitality of the staff and user administration at the NSLS and the National Center for Electron Microscopy for use of its microscopes. We also thank the staff and user administration at SSRL and, in particular, Sean Brennan for his support of beam line 7-2. SSRL is operated by the Department of Energy, Division of Chemical Sciences. Finally we would like to thank Albert Goossens (Technical University, Delft, The Netherlands) and Jack Porter (University of California, Berkeley) for helpful discussion of the interface transition. This work was supported by the Director, Office of Basic Energy Sciences, Materials Sciences Division of the U.S. Department of Energy under Contract No. AC03-76SF00098.

- *Also at Department of Physics, University of California, Berkeley, CA 94720.
- ¹S. Sinharoy, *Thin Solid Films* **187**, 231 (1990).
- ²M. A. Olmstead, R. I. Uhrberg, R. D. Bringans, and R. Z. Bachrach, *Phys. Rev. B* **35**, 7526 (1987).
- ³S. Rieger, F. J. Himpsel, U. O. Karlsson, F. R. McFeely, J. F. Morar, and J. A. Yarmoff, *Phys. Rev. B* **34**, 7295 (1986).
- ⁴R. M. Tromp and M. C. Reuter, *Phys. Rev. Lett.* **61**, 1756 (1988).
- ⁵Ph. Avouris and R. A. Wolkow, *Appl. Phys. Lett.* **55**, 1074 (1990).
- ⁶J. Zegenhagen and J. R. Patel, *Phys. Rev. B* **41**, 5315 (1990).
- ⁷G. C. L. Wong, D. Loretto, E. Rotenberg, M. A. Olmstead, and C. A. Lucas, *Phys. Rev. B* **48**, 5716 (1993).
- ⁸J. D. Denlinger, E. Rotenberg, U. Hessinger, M. Leskovar, and M. A. Olmstead, *Appl. Phys. Lett.* **62**, 2057 (1993).
- ⁹J. L. Batstone, J. M. Phillips, and E. C. Hunke, *Phys. Rev. Lett.* **60**, 394 (1988).
- ¹⁰J. Zegenhagen, *Surf. Sci. Rep.* **18**, 199 (1993); K. G. Huang, J. Zegenhagen, J. M. Phillips, and J. R. Patel, *Phys. Rev. Lett.* **72**, 2430 (1994).
- ¹¹C. A. Lucas, G. C. L. Wong, and D. Loretto, *Phys. Rev. Lett.* **70**, 1826 (1993).
- ¹²C. A. Lucas and D. Loretto, *Appl. Phys. Lett.* **60**, 2071 (1992).
- ¹³A. Ishizaka, T. Doi, and M. Ichikawa, *Appl. Phys. Lett.* **58**, 902 (1991).
- ¹⁴This is higher than our previously reported thermocouple reading at the (7×7)-(1×1) transition (780°C) and we attribute the difference to a different heater/thermocouple arrangement. The transition temperature changed abruptly between the two values as a result of maintenance to the sample manipulator/heater setup.
- ¹⁵P. H. Fuoss and I. K. Robinson, *Nucl. Instrum. Methods* **222**, 171 (1984); I. K. Robinson, in *Handbook on Synchrotron Radiation, Vol. 3*, edited by D. E. Moncton and G. S. Brown (Elsevier, New York, 1991).
- ¹⁶These experiments were performed within days of each other and the deposition rate was approximately constant, as checked by measurements of thicker CaF₂ films. Slight variations in the growth rate have been observed over several months.
- ¹⁷The integrated intensity is the product of the peak height and FWHM as the detector integrates over the radial reciprocal space direction.
- ¹⁸The Si-(7×7) surface reconstruction is well known to be preserved under an amorphous Si cap; see, for example, J. M. Gibson, H.-J. Gossman, J. C. Bean, R. T. Tung, and L. C. Feldman, *Phys. Rev. Lett.* **56**, 355 (1986).
- ¹⁹Since ionic bonding is equivalent to a low-energy packing of charged spheres, it is conceivable that, at low coverages, the fluorine is in more than one chemical environment. The spectrometer resolution does not allow separation of the components in the F spectrum, but the width of the peak is significantly broader than that obtained from thick CaF₂ films.
- ²⁰M. A. Olmstead, R. I. G. Uhrberg, R. D. Bringans, and R. Z. Bachrach, *J. Vac. Sci. Technol. B* **4**, 1123 (1986).
- ²¹G. C. L. Wong, C. A. Lucas, D. Loretto, A. P. Payne, and P. H. Fuoss, *Phys. Rev. Lett.* **73**, 991 (1994).
- ²²R. C. Pond, *CRC Rev. Solid State Mater. Sci.* **15**, 441 (1989). Line defects showing similar contrast have been observed in crystallographically equivalent CoSi₂/Si(111). See, for example, R. T. Tung and F. Schrey, *Appl. Phys. Lett.* **54**, 852 (1989).
- ²³A. Tempel and A. Zehe, *Solid State Commun.* **69**, 151 (1989).
- ²⁴N. S. Sokolov, N. L. Yakovlev, and J. Almeida, *Solid State Commun.* **76**, 883 (1990).
- ²⁵R. M. Tromp, F. K. LeGoues, W. Krakow, and L. J. Schowalter, *Phys. Rev. Lett.* **61**, 2274 (1988).
- ²⁶S. R. Andrews and R. A. Cowley, *J. Phys. C* **18**, 6427 (1985); I. K. Robinson, *Phys. Rev. B* **33**, 3830 (1986).
- ²⁷R. Feidenhans'l, *Surf. Sci. Rep.* **10**, 105 (1989).
- ²⁸I. K. Robinson, R. T. Tung, and R. Feidenhans'l, *Phys. Rev. B* **38**, 3632 (1988).
- ²⁹S. N. G. Chu, A. T. Macrander, K. E. Strege, and W. D. Johnston, *J. Appl. Phys.* **57**, 249 (1985).
- ³⁰T. Nakayama, M. Katayama, G. Selva, and M. Aono, *Phys. Rev. Lett.* **72**, 1718 (1994).
- ³¹I. K. Robinson and D. J. Tweet, *Rep. Prog. Phys.* **55**, 599 (1992).
- ³²For a study of defects in thin epitaxial films and their effect on the specular x-ray scattering, see P. F. Miceli, in *Semiconductor Interfaces, Microstructures and Devices: Properties and Applications*, edited by Z. C. Feng (Hilger, Bristol, 1992).
- ³³The atomic form factors are obtained from polynomial fits to the values given in *The International Tables for X-ray Crystallography, Vol. 3* (Kynoch, Birmingham, England, 1968).
- ³⁴R. G. van Silfhout, J. F. van der Veen, C. Norris, and J. E. Macdonald, *Faraday Discuss. R. Chem. Soc.* **89**, 169 (1990).
- ³⁵W. R. Busing and H. A. Levy, *Acta Crystallogr.* **22**, 457 (1966).
- ³⁶G. Renaud, P. H. Fuoss, J. Bevk, and B. S. Freer, *Phys. Rev. B* **45**, 9192 (1992).
- ³⁷M. F. Toney and D. G. Wiesler, *Acta Crystallogr. Sec. A* **49**, 624 (1993).
- ³⁸Y. Kashiwara, K. Kawamura, N. Kashiwagura, and J. Harada, *Jpn. J. Appl. Phys.* **26**, L1029 (1987).
- ³⁹R. G. van Silfhout, Ph.D. thesis, University of Leiden, 1991.
- ⁴⁰M. Y. Gamarnik, *Phys. Status Solidi B* **172**, K51 (1992).
- ⁴¹In TEM samples prepared from thicker CaF₂ layers, a thicker residual Si substrate is needed to prevent the strained CaF₂ from relaxing. This increases the diffuse background.
- ⁴²D. Cherns, *Philos. Mag. B* **30**, 549 (1974).
- ⁴³F. M. Ross and J. M. Gibson, *Phys. Rev. Lett.* **68**, 1782 (1992).
- ⁴⁴G. Lempfuhl and C. E. Warble, *Ultramicroscopy* **19**, 135 (1986).
- ⁴⁵D. Loretto, F. M. Ross, C. A. Lucas, and G. C. L. Wong, *Appl. Phys. Lett.* (to be published).
- ⁴⁶D. J. Lockwood (private communication).
- ⁴⁷V. Chakarian, T. D. Durbin, P. R. Varekamp, and J. A. Yarmoff, *Phys. Rev. B* **48**, 18332 (1993).
- ⁴⁸Prolonged exposure to the x-ray beams in our experiments did not drive, or noticeably speed up, the transition.
- ⁴⁹W. Weiss, H. D. Wiemhöfer, and W. Göpel, *Phys. Rev. B* **45**, 8478 (1992).
- ⁵⁰R. T. Tung and J. P. Sullivan (private communication).

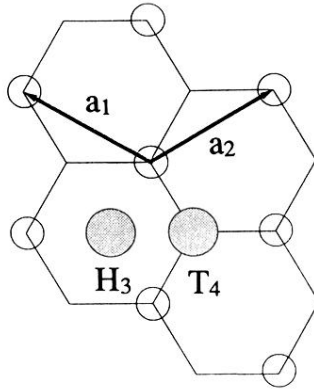


FIG. 11. Top view of the Si surface unit cell. The two possible adsorption sites T_4 and H_3 for the Ca atom in the CaF layer at the interface are shown by the shaded atoms. The basis vectors of the hexagonal unit cell are indicated.

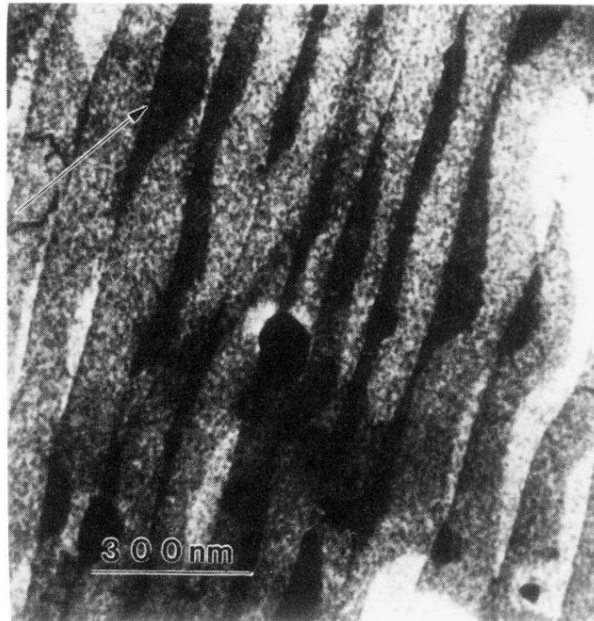


FIG. 12. TEM micrograph, imaged with CaF_2 $[11\bar{1}]$, from a $\text{CaF}_2/\text{Si}(111)$ film deposited at a substrate temperature $T=770^\circ\text{C}$ to a thickness of approximately five CaF_2 triple layers. The diffraction vectors are marked and the scale bar is $0.5\ \mu\text{m}$ long. The incident beam direction is close to $[123]$. Changes in thickness of one CaF_2 triple layer ($\frac{1}{3}[111]$) appear as a change in brightness of the image. $\frac{1}{3}[111]$ steps at the interface, which are correlated with the array of line defects seen in Fig. 5(b), are visible, as are the $\frac{1}{3}[111]$ steps at the CaF_2 surface.

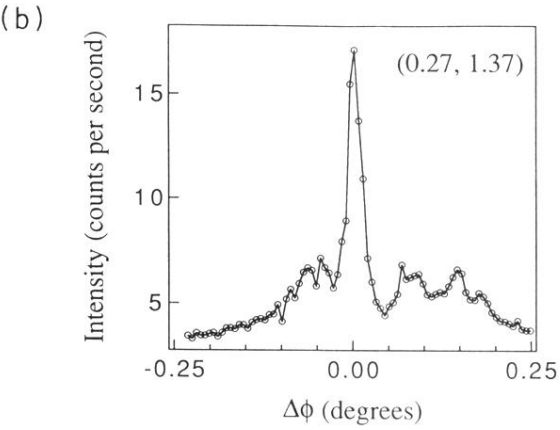
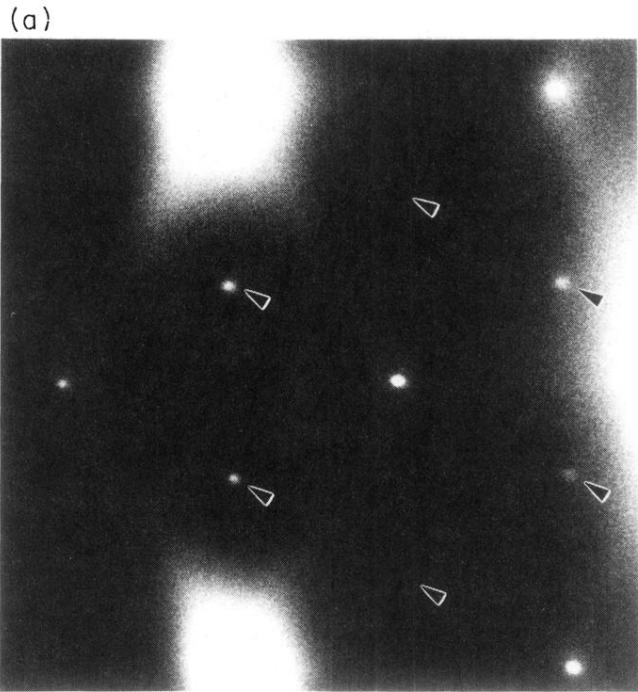


FIG. 14. (a) Part of a [111] transmission-electron-diffraction pattern from an 18 triple-layer-thick CaF_2 film. The features marked with arrows lie close to $\frac{1}{3}\langle 220 \rangle$ positions and can be attributed to a reconstructed layer at the $\text{CaF}_2/\text{Si}(111)$ interface, with a $(\sqrt{3} \times \sqrt{3})R 30^\circ$ symmetry, indexed using the Si unit cell. (b) A grazing incidence x-ray rocking scan at $(0.27, 1.37, 0.05)$ in the reciprocal lattice notation defined in Eq. (2). For a commensurate $(\sqrt{3} \times \sqrt{3})R 30^\circ$ reconstruction there would be a peak at $(\frac{1}{3}, \frac{4}{3}, 0)$. The peak center is displaced away (a rotation of $\sim 1.9^\circ$) from the commensurate position. The solid line is a guide to the eye.

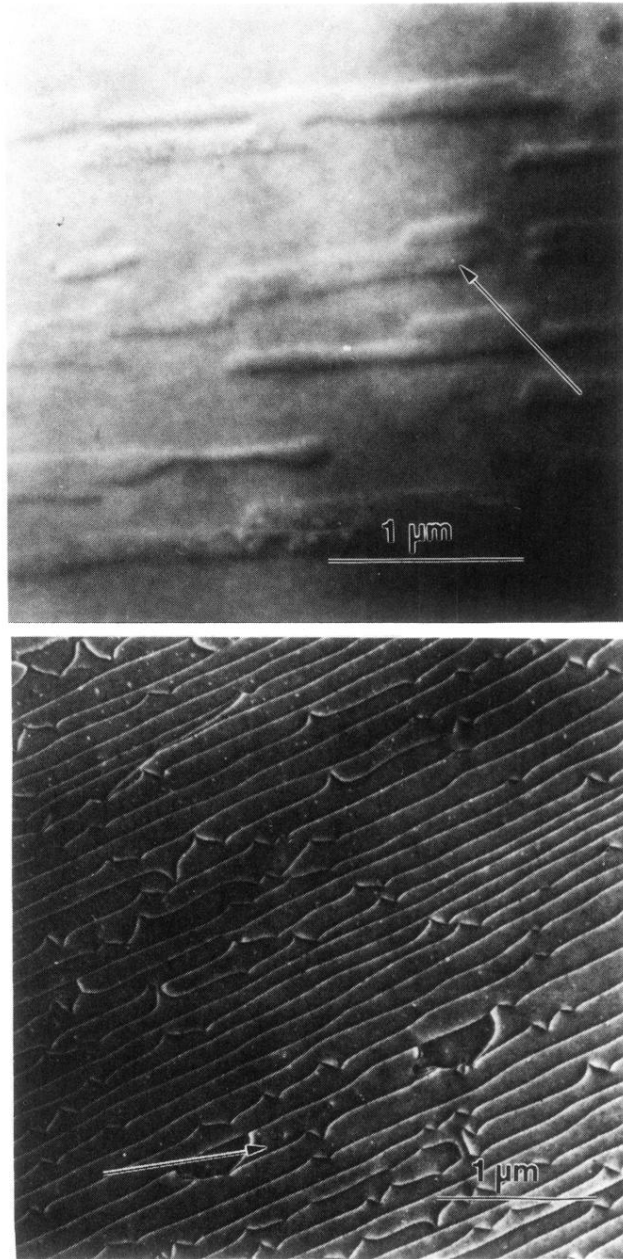


FIG. 5. TEM images taken from $\text{CaF}_2/\text{Si}(111)$ samples. (a) Bright-field image after 8 sec of CaF_2 deposition at $T=550^\circ\text{C}$. (b) Dark-field image after 100 sec of CaF_2 deposition at $T=700^\circ\text{C}$. The appropriate $\langle 220 \rangle$ diffraction vectors are marked.

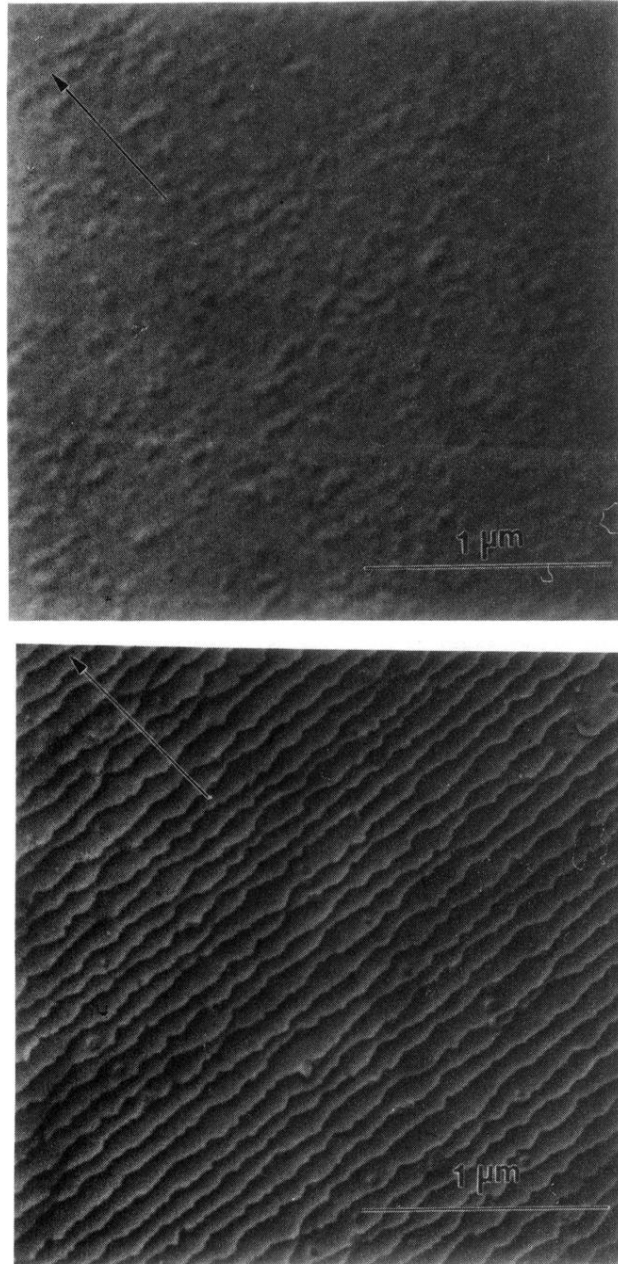


FIG. 6. Dark-field TEM images taken from $\text{CaF}_2/\text{Si}(111)$ samples grown at $T=450^\circ\text{C}$ (a) after 5 sec of CaF_2 deposition and (b) after 100 sec of CaF_2 deposition. The appropriate $\langle 220 \rangle$ diffraction vectors are marked.

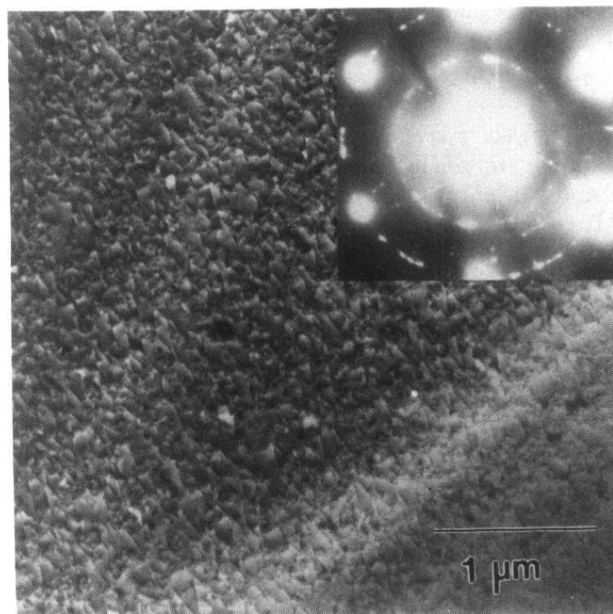


FIG. 7. Dark-field TEM image taken from a $\text{CaF}_2/\text{Si}(111)$ sample after 100 sec of deposition at room temperature. The inset is the $[111]$ transmission-electron-diffraction pattern from the same sample, taken at 200 keV. The pattern shows rings associated with the polycrystalline CaF_2 .

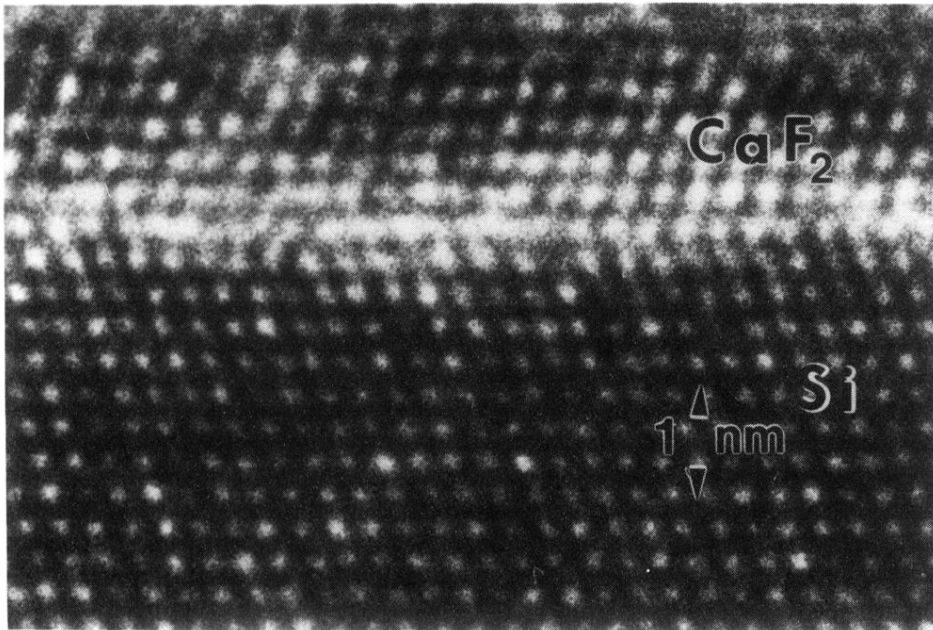


FIG. 8. High-resolution TEM image of the $\text{CaF}_2/\text{Si}(111)$ interface along the Si $[1\bar{1}0]$ direction, in a sample grown at $T=720^\circ\text{C}$ and determined to be approximately nine CaF_2 triple layers ($\sim 30 \text{ \AA}$) thick. The point to point resolution is approximately 0.24 nm . The twin orientation (B -type stacking) of the CaF_2 film is readily apparent.